

Experimental study on high cycle fatigue performance and damage mechanism of welded tubular structures with butt joints

Yanlin Guan^{1a}, Yaqiang Yang^{*1}, Wenping Du^{1b}, Mohamed F.M. Fahmy^{2c}, Haitao Wang^{3d} and Jing Cui^{4e}

¹Dept. of Civil Engineering, School of Architecture and Civil Engineering, Jiangsu University of Science and Technology, Zhenjiang, 212100, China

²Dept. of Civil Engineering, Faculty of Engineering, Assiut University, Assiut, 71516, Egypt

³Dept. of Civil Engineering, College of Civil and Transportation Engineering, Hohai University, Nanjing, 210098, China

⁴Dept. of Civil Engineering, College of Civil Engineering and Architecture, Henan University of Technology, Zhengzhou, 450001, China

(Received January 9, 2025, Revised September 9, 2025, Accepted October 14, 2025)

Abstract. Based on high-cycle fatigue tests and microstructural analysis, the fatigue performance and fracture failure mechanisms of butt joints in welded tubular structures were investigated. According to static behavior of the butt joints, high-cycle fatigue experiments were carried out at different stress levels. A life prediction model for butt joints of welded tubular structures under high-cycle fatigue load was proposed by introducing Morrow stress-life fatigue curve. With fracture micro-morphology analysis, the fracture failure mechanism of butt joints in welded tubular structures was revealed. The experiment results indicate that the welded tubular structure exhibited brittle damage at the weld seam under fatigue loading. The test was cycled 2 million times under the stress ratio $R = 0.1$, and the fatigue strength was 156.29MPa. The resulting fatigue life prediction formula demonstrated good agreement with the experimental results. Based on the fatigue experimental results, the fatigue life prediction model applied to high-cycle fatigue was established. With a large number of fatigue striations in the crack propagation zone, the fatigue fracture was smooth and neat at the crack source, while the final fracture zone occupied a small proportion of the fracture plane.

Keywords: butt joints; fatigue life; high-cycle fatigue testing; partial strain fatigue analysis; welded tubular structures

1. Introduction

Welded tubular structures refer to a type of steel structure where part or all of the components of the structural system are composed of circular steel tubes connected in different joining techniques. Due to their lightweight, reliable connections, and convenient construction, they are widely used in large venues, airports, stations, offshore platforms, and other fields (Guo *et al.* 2018, De Oliveira *et al.* 2008, Zou *et al.* 2025a, 2025b, Jiang *et al.* 2025).

However, with the deterioration of the working environment and the increase in service time, the fatigue failure phenomenon of welded tubular structures is becoming increasingly serious (Yang *et al.* 2022, Musa and Mashiri 2019). As a key part of the connection in welded tubular structures, the weld has become a weak link under fatigue load due to adverse factors such as welding defects (Fu *et al.* 2016, Haedir *et al.* 2009, Tong *et al.* 2019, Smith and Smith 1982, Barsoum and Samuelsson 2006), residual stress (Zhao and Packer 2000, Marshall 2013), heat-affected zone (Chen *et al.* 2004), geometric deformation (Gurney 1991, Nussbaumer and Costa Borges 2008), and so on. The fatigue performance of the weld in welded tubular structures directly affects the long-term service safety of the

welded tubular structures. Therefore, the study of the fatigue performance of the welded connections in welded tubular structures is of great significance to ensure the safety and durability of welded tubular structures.

Based on the different welding connection methods, welded tubular structures can be divided into lap joints, T-joints, Y-joints, K-joints, and butt joints. In both the API (Digre and Zwerneman 2012) and DNV (DNV-RP-C203 2011) standards, S-N curves for the fatigue life of tubular joints are provided. Numerous studies have been conducted by scholars from various countries to investigate the fatigue performance of welded tubular structures with different connection methods. Jin *et al.* (2023) employed submerged arc welding to join T-shaped lap joints of SW400 fine-grain high-strength steel. They conducted radial fatigue tests using various welding parameters to investigate the influence of welding processes on weld geometry and joint fatigue performance. Scanning electron microscopy was used to analyze fatigue fracture morphology. The study revealed that crack initiation occurred very early, predominantly in the high-stress region near the center of the weld seam. This suggests the need for further optimization of welding techniques in practical applications to extend the structural service life. Wang *et al.* (2023) simulated the welding temperature field and residual stress distribution of T-shaped and Y-shaped Q355 tubular truss structures during multi-layer multi-pass manual arc welding using finite element software. The study revealed that both types of welded tubular structures exhibited an asymmetric

*Corresponding author, Ph.D. Associate Professor
E-mail: yangyq@just.edu.cn

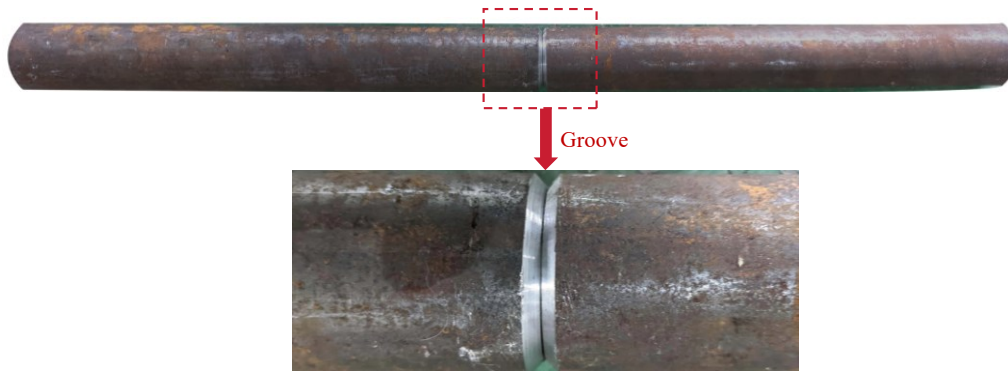


Fig. 1 Seamless steel tube before welding



Fig. 2 Seamless steel tubular after welding

and non-uniform temperature field during the welding process. These findings highlight the importance of considering welding parameters and techniques to optimize the performance and reliability of such structures in practical applications. Yan *et al.* (2020) studied the influence of adding reinforcement plates in K-shaped welded joints of circular tubes on hysteresis performance through quasi-static tests. The experiments found that reinforcing the joint with plates effectively increased its load-bearing capacity and delayed the plastic deformation of the main tube. Shao *et al.* (2020) and Li *et al.* (2022) conducted static load tests on T-shaped welded joints reinforced with CFRP to study their ability to reduce deformation under axial compression and improve stiffness and load-bearing capacity. Acevedo *et al.* (2011, 2012a, 2012b, 2013) conducted a study on the fatigue performance of K-shaped welded tubular structures in truss highway bridges using experimental and numerical methods. Through crack propagation simulation analysis, the influence of residual stress was investigated. Based on the impact of welding residual stress, an analytical equation for residual stress distribution was proposed to provide information on the trend of residual stress related to joint geometry, which helped optimize design to reduce the risk of fatigue cracks and improve structural safety and service life. Lee *et al.* (2013, 2014a) conducted an in-depth discussion on the pressure-bearing and bending resistance capabilities of ring butt-welded structures, analyzing the impact of welds on the load-bearing capacity of ring structures. The research showed that as the ratio between diameter and thickness increased, there was an increase in the reduction degree for pressure bearing capacity in ring welding structures. In addition, Lee and Chang (2014b) compared residual stresses and deformation characteristics between austenitic stainless steel and duplex stainless steel ring butt-welded structures, finding that the differences in thermodynamic properties of materials led to an asymmetric

distribution of residual stresses in weld seams. Furthermore, larger welding residual stresses were observed on the side of the welded component exhibiting higher yield strength.

Compared with flange connection and T-joint connection, butt joint connection not only had the advantages of simple process and material saving, but also could achieve connections at different angles. It was widely used for connecting tubes with various diameters and wall thicknesses (De Oliveira *et al.* 2008, Haldimann-Sturm and Nussbaumer 2008, Nussbaumer *et al.* 2006). However, due to the complex fatigue failure mechanism of welded tubes and numerous influencing factors, there was limited research on the high cycle fatigue performance of welded tubular structures and methods for predicting their fatigue life under high cycle fatigue. Therefore, it was urgent to carry out research on the fatigue performance of welded tubular structures to promote their widespread application. In this paper, static mechanical performance tests and high-cycle fatigue tests were conducted on the butt joints of welded tubular structures. The degradation law of fatigue performance was analyzed based on digital image technology and experimental results. A fatigue life prediction model for welded tubular structures was proposed by introducing Morrow stress-life fatigue curve correction to the Manson-Coffin equation. Furthermore, microscopic studies on fracture morphology were combined to reveal the fatigue failure mechanism of butt joints in welded tubular structures under high-cycle fatigue conditions.

2. Experimental program

2.1 Specimen design

The test specimens were fabricated using a seamless Q345 steel tube, with an inner diameter of 40 mm and an

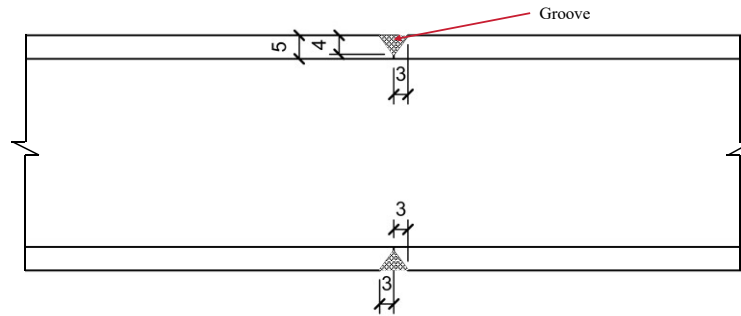


Fig. 3 Steel tubes groove setting diagram (Unit: mm)

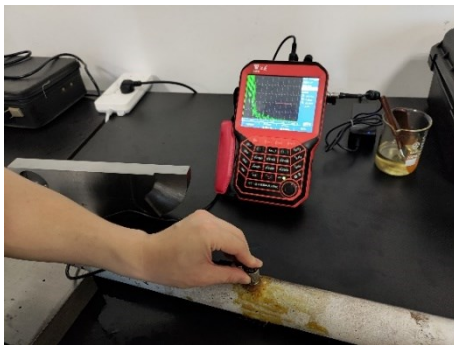


Fig. 4 Weld quality inspection



Fig. 5 Tensile test setup

Table 1 Chemical Composition of Welding Wire (%)

Element	C	Mn	Si	S	P	Cu	Total of Other Elements
Standard Value	0.05-0.12	1.20-1.50	0.60-0.85	≤0.025	≤0.025	≤0.30	≤0.50

Table 2 The welding process parameters

Welding process	Welding current (A)	Arc voltage (V)	Welding speed (mm/min)	Argon gas flow rate (L/min)	Preheating temperature (°C)	Interlayer temperature (°C)
Base welding	85~95	10~12	80~90	12~15	80~100	≤150
Filler welding	110~120	13~15	100~110	15~18	-	≤150
Cover welding	95~105	12~14	90~100	15~18	-	≤150

outer diameter of 50 mm. Each tubular segment had a length of 400 mm. The welding wire selected for the steel tube was an argon arc welding wire (Model: TIG-50-6), whose chemical composition is presented in Table 1. Argon (Ar) gas, with a purity of 99.99%, was used as the shielding gas during welding. Pre-deformation measures and preheating were applied before welding. Post welding, the implementation of heat retention measures was essential to ensure uniform cooling of the welded components, thereby preventing uneven deformation, the welding process parameters are shown in Table 2. Before and after welding were shown in Figs. 1 and 2, and groove setting were shown in Fig. 3. After welding, the welding quality was basically confirmed by ultrasonic detection, as shown in Fig. 4.

2.2 Static test methods

Mechanical properties of unwelded steel tubes and

welded steel tubes at room temperature were tested via unidirectional tensile test according to ASTM E8/E8M-2013a (ASTM 2013), which specifies tensile test methods for metallic materials. To avoid large deformation of the steel tubes during the clamping process, steel rods were filled in the clamping ends of the steel tubes on the testing machine. The test apparatus used was a 2000kN electro-hydraulic servo universal testing machine with a loading speed of 3mm/min, and the test setup is shown in Fig. 5.

2.3 Fatigue test methods

According to the requirements of "ASTM E466-2015 Standard Practice for Conducting Force-Controlled Constant Amplitude Axial Fatigue Tests of Metallic Materials" (ASTM 2015), fatigue tests were conducted using a load control form of constant amplitude sinusoidal wave (as shown in Fig. 6(a)). The frequency was set at 12Hz and the stress ratio R was 0.1, where $R = P_{min} / P_{max}$

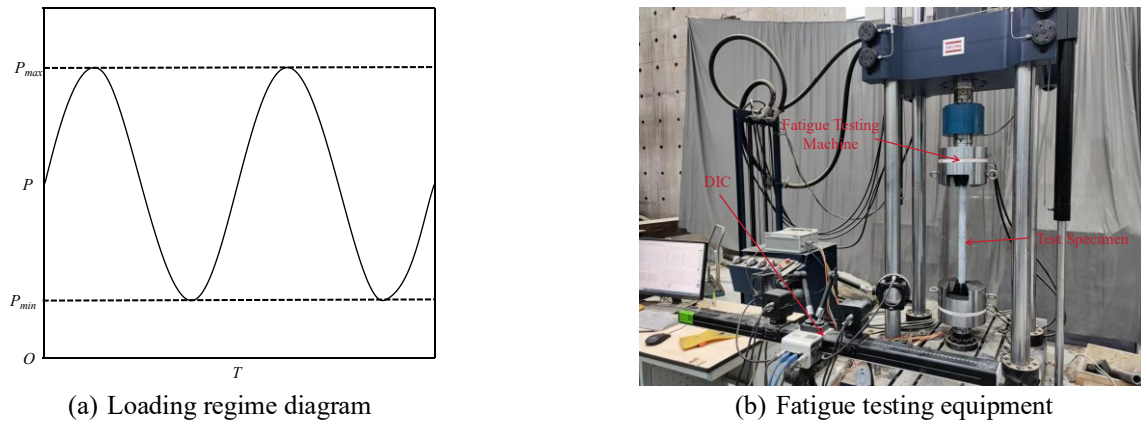


Fig. 6 Loading amplitudes and fatigue testing apparatus

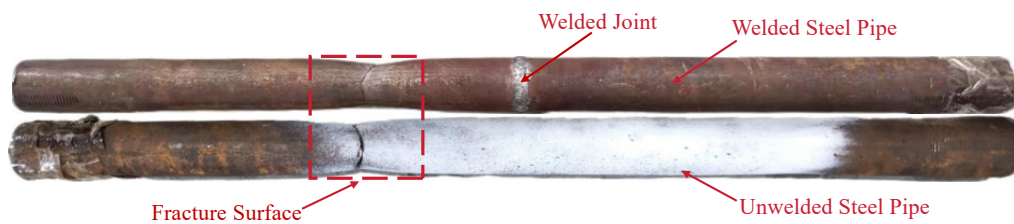


Fig. 7 Failure morphology of unwelded and welded steel Ttubes

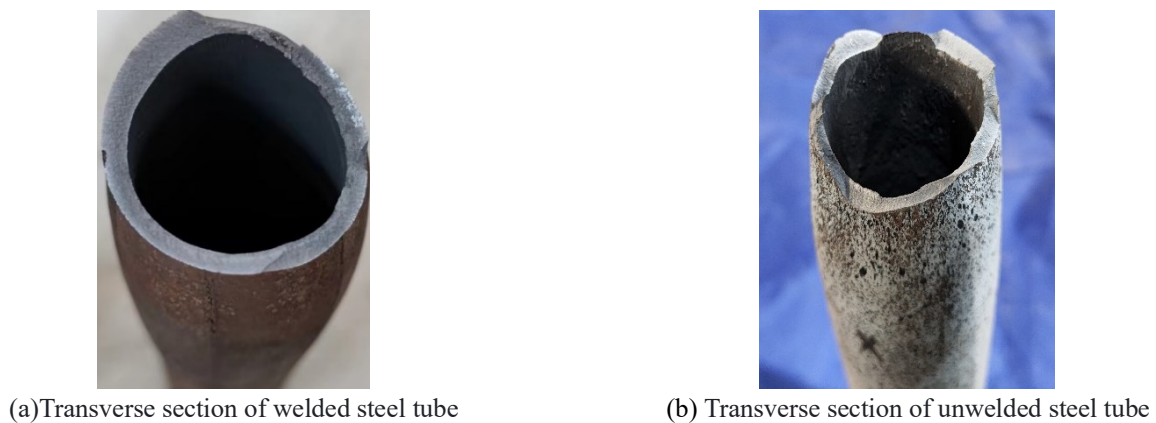


Fig. 8 Cross-sections at the failure locations

(P_{min} was the minimum load and P_{max} was the maximum load). The fatigue tests were carried out in descending order of stress amplitude converted by loading coefficient K from large to small ($K = P_{max} / P_y$, where P_y was the yield load of welded steel tube). The initial maximum load amplitude for testing was set at $0.7P_y$, followed by gradually decreasing loading coefficients with a tolerance of 0.05. If the specimen had not fractured after reaching 2 million cycles, the loading will be stopped. The loading conditions were shown in Table 3. The fatigue test system consists of a 500kN fatigue testing machine and a three-dimensional full-field strain measurement and analysis system as shown in Fig. 6(b)

3. Static test results

The ultimate failure modes of unwelded steel tubes and

welded seam tubes are shown in Figs. 7 and 8. From Fig. 7, the failure patterns of both are consistent. The steel tubes exhibit an obvious necking phenomenon during uniaxial tensile tests, with the failure occurring at a distance of 150 mm from the center. Fig. 8 shows that the fracture surfaces are relatively smooth and cup-conical in shape. The results of uniaxial tensile tests for unwelded steel tubes and welded seam tubes are presented in Table 4. Compared to unwelded steel tubes, the yield strength of welded seam tubes decreases by 0.2% while the tensile strength increases by 0.6%. This indicates that there is no significant deterioration in mechanical properties due to welding; thus, the mechanical performance of materials remains similar before and after welding. The stress-strain curves, as shown in Fig. 9, demonstrate that both unwelded steel tubes and welded seam tubes undergo the elastic stage, strengthening stage, and failure stage without a distinct yield point. In comparison to unwelded steel tubes, the elastic modulus of

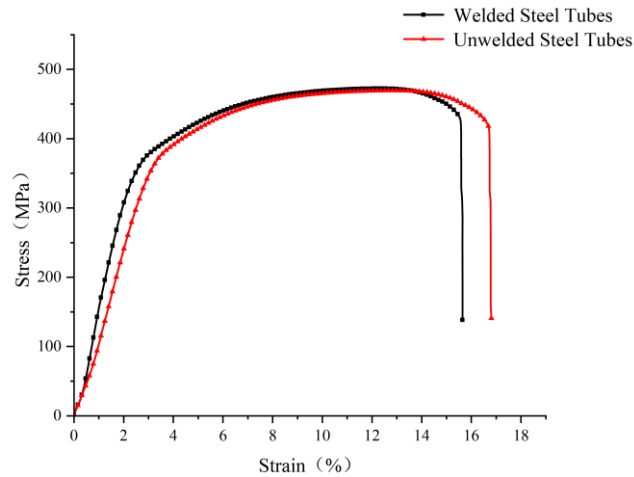


Fig. 9 Stress-strain curves

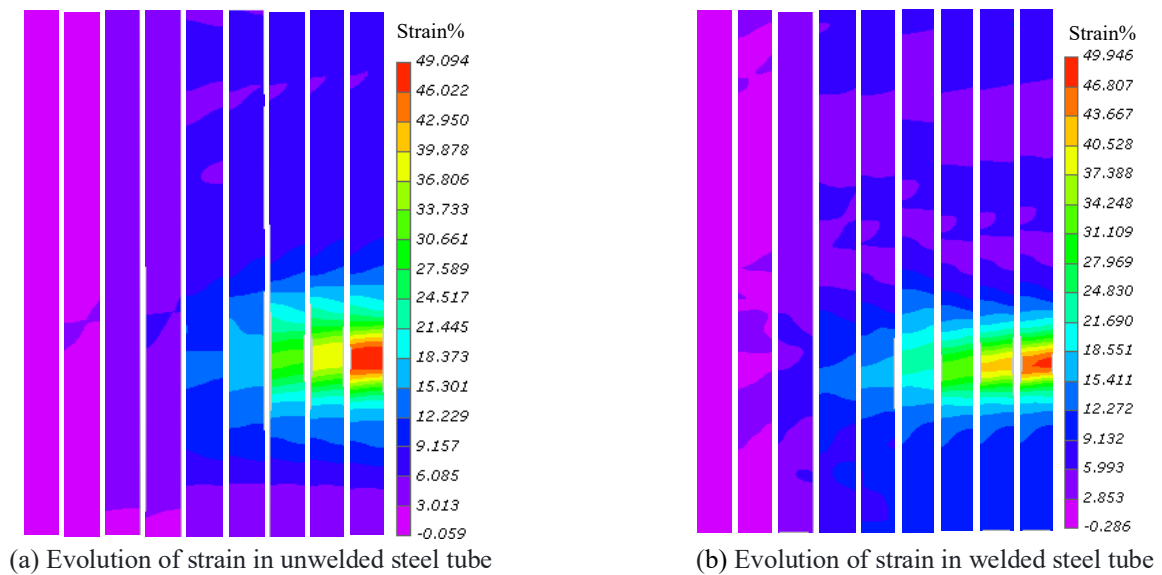


Fig. 10 Evolution of strain in unwelded and welded steel tubes under uniaxial tension

Table 3 Loading Conditions

Loading coefficients(K)	Maximum load (kN)	Minimum load (kN)	Maximum stress (MPa)	Frequency (Hz)
0.7	171.850	17.185	243.12	12
0.65	159.575	15.958	225.75	12
0.6	147.300	14.730	208.39	12
0.55	135.025	13.503	191.02	12
0.5	122.750	12.275	173.66	12
0.45	110.475	11.048	156.29	12

welded seam tubes increases by 3.76%, possibly due to reduced plastic deformation caused by high-strength welding wire material used in their construction leading to an increase in their elastic modulus.

Using Digital Image Correlation (DIC) technology, the strain patterns of both unwelded and welded steel tubes under uniaxial tensile loading were analyzed (as shown in

Fig. 10). The camera resolution of the DIC system was 2448×2048 pixels, with a pixel size of $3.45 \mu\text{m}$. From Fig. 10, it can be observed that as the load gradually increases, the overall strain of the steel tube in tension increases. Since the testing machine primarily applies tension by moving downwards from the lower fixture located on a crossbeam, when the load reaches the yield point of the steel tube,

Table 4 Mechanical Properties

Specimen Name	Yield Strength f_y (MPa)	Ultimate Tensile Strength f_u (MPa)	Elastic Modulus E_a ($\times 10^5$ MPa)	Failure Mode
Unwelded Steel Tubular	348.0	469.8	1.86	Ductile Fracture
Welded Steel Tubular	347.3	472.7	1.93	Ductile Fracture

Table 5 Fatigue test results

Loading coefficients (K)	Fatigue cycles (N_f)	Maximum displacement difference (ΔD) (mm)	Failure mode
0.7	88960	1.11	Weld Seam Fracture
0.65	291960	1.06	Weld Seam Fracture
0.6	377580	0.95	Weld Seam Fracture
0.55	646220	0.90	Weld Seam Fracture
0.5	832060	0.81	Weld Seam Fracture
0.45	2000000	0.78	Undamaged



Fig. 11 Fatigue fracture surfaces

strains concentrate in the lower half of the tube. The overall strain distribution is relatively uniform for unwelded steel tubes, while for welded steel tubes, due to higher welded wire strength, strains at welding locations decrease, and stresses concentrate in the lower half of the tube.

4. Fatigue test results and analysis

The results of the fatigue test indicated that the fatigue fractures of the specimens occurred at the weld seam, without evident necking phenomenon. The surface morphology of the edge instantaneous fracture zone was relatively rough and exhibited a tearing distribution pattern. This type of failure mode belonged to brittle fracture, which was caused by localized heating and rapid cooling during the welding process, resulting in uneven thermal expansion and contraction. Consequently, highly concentrated residual stress could be generated in and around the weld seam, potentially surpassing the material's yield strength under externally applied fatigue load and leading to crack initiation. Additionally, internal or surface defects such as

pores, slag inclusions, and microcracks might have existed during welding process, thereby reducing carrying capacity and serving as starting points for fatigue cracks. Moreover, filling welding materials had the potential to alter microstructure and mechanical properties within the welded area, inducing increased hardness but decreased toughness along with enhanced sensitivity ultimately contributing to weld damage (as depicted in Fig. 11).

The results of the fatigue test are shown in Table 5. As the loading coefficient K decreased, the number of fatigue cycles increased, and the maximum displacement of the specimen decreased. When the loading coefficient was 0.45, there was no failure in the welded joint structure after two million fatigue cycles, indicating that the fatigue strength of the welded joint structure to butt joints was $0.45f_y$. The upper and lower limit displacements of the welded joint structure under fatigue load are shown in Fig. 12. From Fig. 12, it could be seen that with an increase in fatigue cycles, both maximum and minimum displacements gradually increased while their difference decreased with a decrease in stress amplitude.

Before the fatigue test, matte white background with black

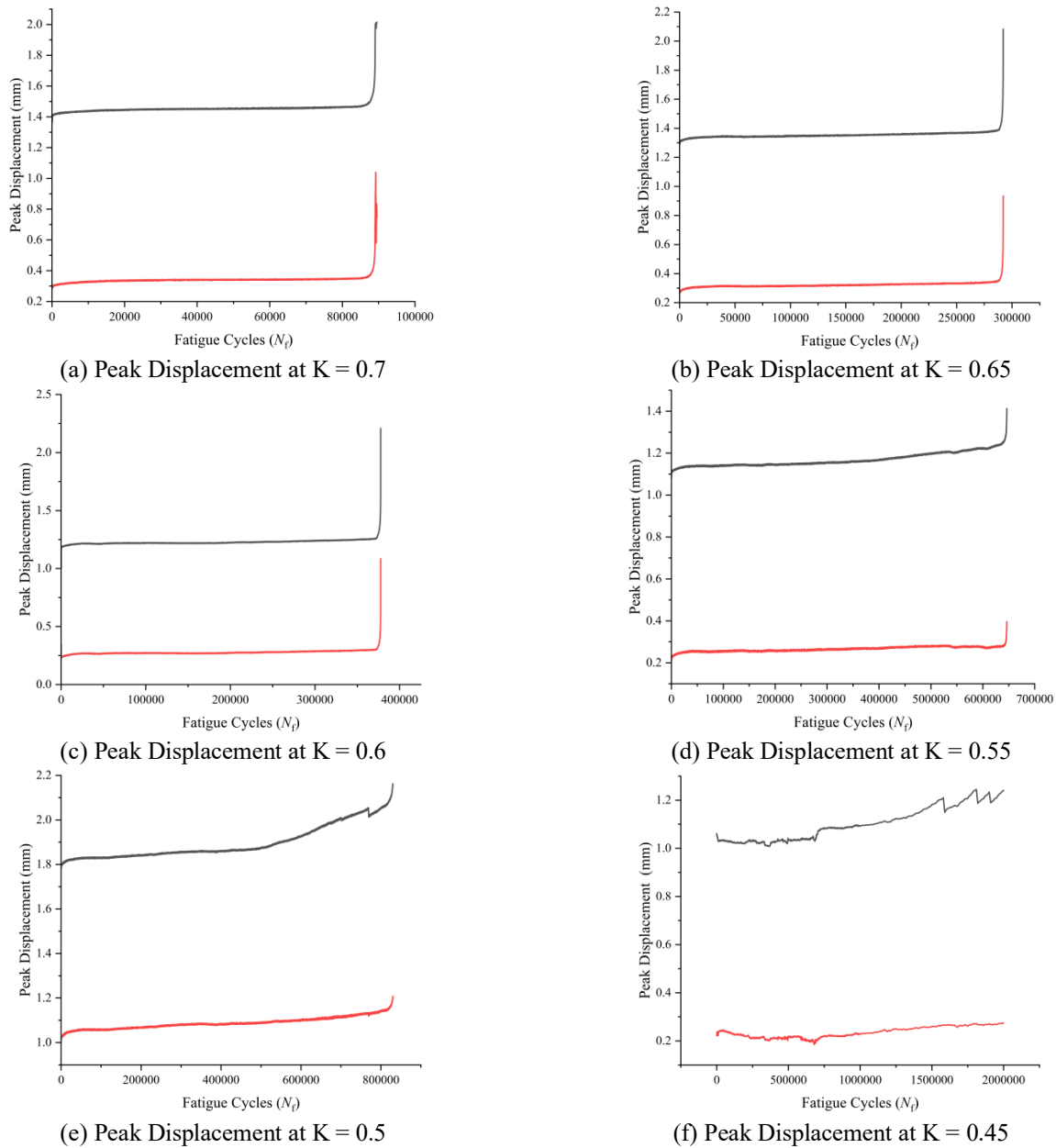


Fig. 12 Variation of peak displacements under different loading coefficients

dot array speckles (with a spot diameter of 50 to 80 μm and a density of ≥ 30 spots/ mm^2) were prepared at the weld toe and the heat-affected zones on both sides of the butt joint specimens to ensure that the speckle contrast met the DIC measurement accuracy requirements (displacement measurement error ≤ 0.01 mm). Two industrial cameras with a resolution of 2448×2048 pixels were used to synchronously capture the speckle images during the cyclic loading process at a sampling frequency of 5 Hz. Strain data were extracted at the 100th loading cycle to avoid errors caused by the instability of the initial loading. The maximum strain in the observation area was calculated using commercial DIC analysis software (XTDIC).

By utilizing DIC technology, the fatigue test process of the welded tubular structure's butt joint was analyzed to study the variation of strain. The evolution of strain under different stress amplitudes is shown in Fig. 13. It can be

observed from the figure that the strain cloud map exhibits symmetry, with maximum strain near the contact area of the weld. Subsequently, it gradually decreases towards both ends. The cross-section in the middle segment of the specimen has a constant value of strain. However, due to significant relative displacement in the weld area, additional tensile (compressive) stress is generated near the contact area as a result of constrained deformation, making it the region with maximum strain.

According to Fig. 13, the maximum strain occurs in the weld area, and the strain values gradually decrease away from the weld area. During the cyclic loading process, fatigue damage accumulates continuously. When crack propagation reaches a critical state, the specimen undergoes brittle fracture. Through DIC analysis, the maximum strain of each specimen can be obtained, as shown in Table 6.

Table 6 The maximum strain of each specimen obtained by DIC

Loading Factor	0.7	0.65	0.6	0.55	0.5	0.45
Maximum Strain (%)	8.366	6.891	5.496	4.814	4.743	3.137

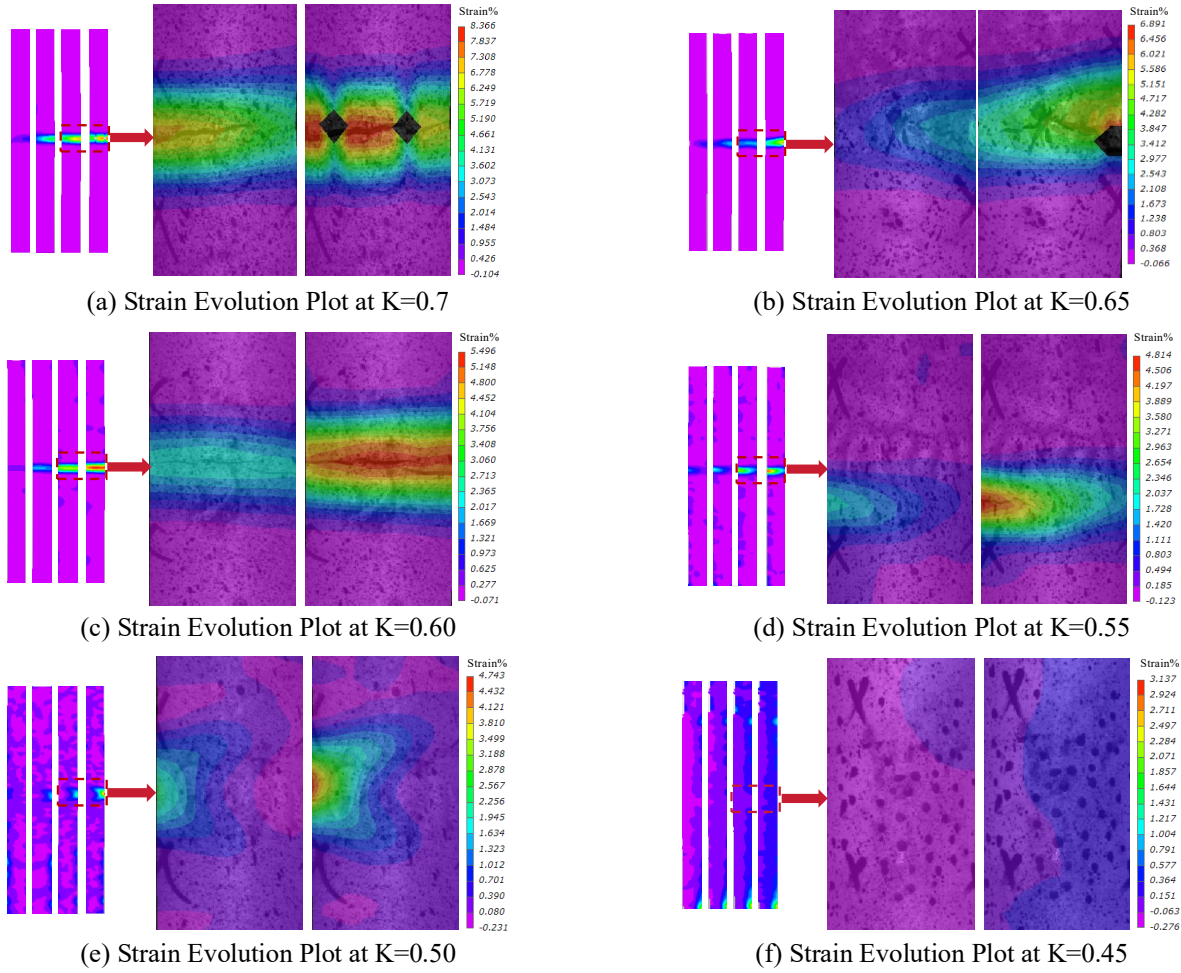


Fig. 13 Strain Evolution under Various Loading Coefficients

5. Fatigue strength curve

5.1 The S-N curve

The S-N curve for the fatigue strength of welded tubular structure butt joints was determined using the Basquin model (Wu *et al.* 2021).

$$S^m N = C \quad (1)$$

where S was the maximum stress and C and m are the performance parameters of the structure or materials. After taking the logarithm of both sides of Eq. (1), obtain an expression for applicability:

$$\lg N = \lg C - m \lg S \quad (2)$$

The S-N curves at 5% and 95% guarantee rates were shown in Eq. (3).

$$\lg N = -m \lg S + \lg C \pm 1.645\sigma \quad (3)$$

Where σ is the standard deviation. The fatigue test data points were fitted, and the S-N curve was illustrated in Fig. 14. The S-N curve for the welded tubular structures with butt joints specimens was shown in Eq. (4), exhibiting an R-squared value of 0.923. It was observed that the fitted curve aligned well with the fatigue test data; as the stress level decreased, the fatigue life increased. All test data points fell within the 95% and 5% confidence intervals, indicating that the error associated with the fitted curve was minimal.

$$\lg N = -6.5972 \lg S + 20.8145 \quad (4)$$

5.2 Prediction method for the service life of butt joints in welded tubular structures

The fatigue crack initiation in welded tubular structures originated from stress concentration areas and gradually expanded under repeated loading. The prediction of fatigue life required the assessment of fatigue damage through

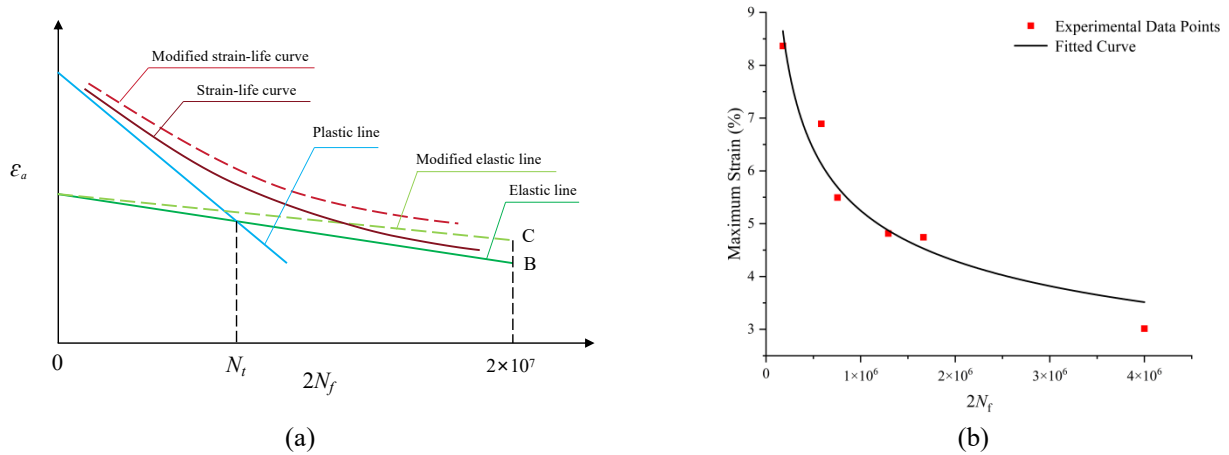


Fig. 15 Strain-Life Curve

Table 7 Comparison of fatigue cycle times and fitting values

Loading coefficients (<i>K</i>)	Number of Experimental Cycles(<i>N</i>)	Maximum Stress – Fitted Value of Cycles (<i>N</i> ₁)/Eq. (4)	Maximum Strain – Fitted Value of Cycles (<i>N</i> ₂)/Eq. (7)
0.7	88960	118780	100430
0.65	291960	193700	194170
0.6	377580	328400	425630
0.55	646220	583130	674320
0.5	832060	1093330	708750
0.45	2000000	2191270	2000000

quantifying local stress and strain states. In comparison to traditional methods, the steady-state local stress-strain approach was able to capture the key areas of fatigue crack initiation and propagation, quantify the local stress and strain state in stress concentration regions, and accurately predict the fatigue life of welded tubular structures.

The Basquin and Manson-Coffin models (Smith *et al.* 1970, Coffin 1954) were expressed as shown in Eq. (5), and the expressed strain-life relationship was shown in Fig. 14(a).

$$\epsilon_a = \epsilon_e + \epsilon_p = \frac{\sigma'_f}{E} (2N_f)^b + \epsilon'_f (2N_f)^c \quad (5)$$

Where, ϵ_a is the the maximum strain, σ'_f is the fatigue strength coefficient, E is the elastic modulus of the material, b is the fatigue strength exponent, ϵ_e is the elastic strain amplitude, ϵ_p is the plastic strain amplitude, ϵ'_f is the fatigue plastic coefficient, c is the fatigue plasticity index, N_f denotes the number of fatigue cycles until failure.

This study employs the Morrow stress-life fatigue curve corrected Manson-Coffin Eq. (40) to calculate the crack initiation life of welded tubular structures, taking into account the mean stress(σ_m) correction. Eq. (1) can be regarded as the case where the mean stress of the corrected equation was zero, and its complete expression was shown in Eq. (6).

$$\epsilon_a = \frac{\sigma'_f - \sigma_m}{E} (2N_i)^b + \epsilon'_f (2N_i)^c \quad (6)$$

This article established a fatigue performance prediction model for welded tubular structures based on the results of fatigue tests on weld joints using the steady-state local stress-strain method. The total strain amplitude ϵ_a in the prediction model was taken from the maximum strain of fatigue tests at different stress levels, which were obtained through DIC analysis as shown in Table 5. The fatigue cycle number N_f was taken from the number of fatigue test cycles, as shown in Table 4. Based on the experimental data, the values of σ'_f , b , ϵ'_f and c were obtained by fitting with the method of least squares and were 227.796, -2.372, 285.594, and -0.289, respectively. Therefore, the fatigue life prediction formula for the butt joint of the welded tubular structure was shown in Eq. (7).

$$\epsilon_a = \frac{227.796 - \sigma_m}{E} (2N_i)^{-2.372} + 285.594 (2N_i)^{-0.289} \quad (7)$$

Based on Eq. (7), the strain-life curve of the butt joint of the welded tubular structure was obtained. The distribution of the strain-life curve and fatigue test data points is shown in Fig. 15(b). From Fig. 15(b), it could be seen that the test data points were evenly distributed on both sides of the fitted curve, with an R-square value of 0.94, indicating a good fit. This suggested that the fatigue life prediction formula proposed in this paper could accurately predict the fatigue performance of the butt joints in welded tubular structures. The current research suffered from limitations due to its reliance on a limited number of samples and specific types of steel and welding materials. It was

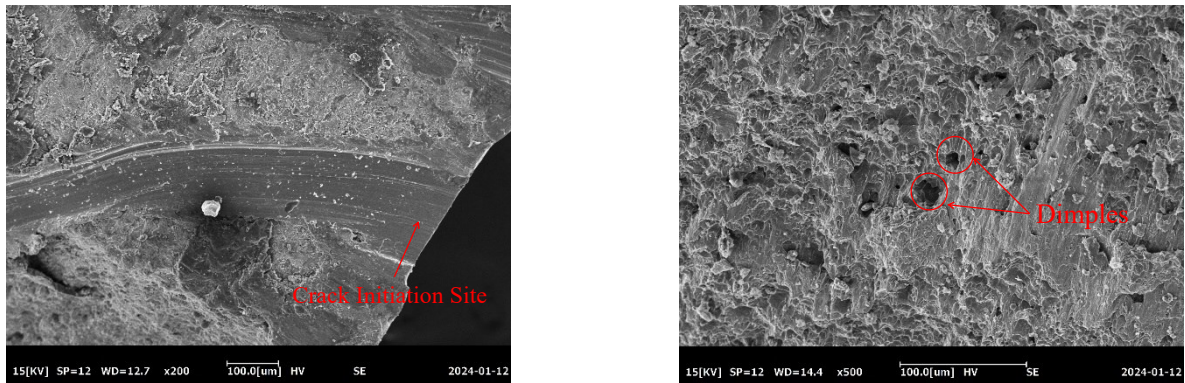


Fig. 16 Fracture Surface under Uniaxial Tension

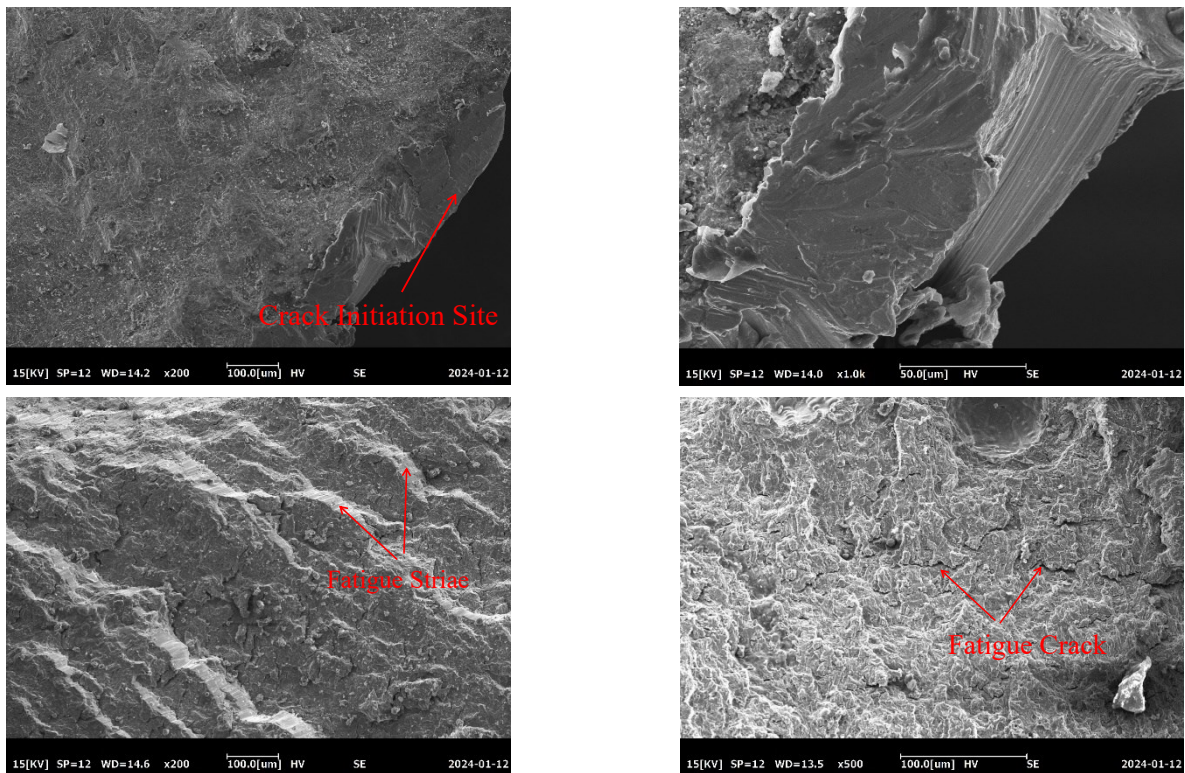


Fig. 17 Microscopic view of fatigue fracture surface

necessary to increase systematic experimental studies to ensure the potential application of the proposed analytical model in designing such welded tubes.

Table 6 presented the experimental values of fatigue cycle counts alongside the fitted values derived from two predictive curves. As indicated in Table 7, the error associated with the S-N curve fitting was found to be 20.23% when compared to the experimental values, whereas the error for the strain-life curve fitting was only 13.05%. Therefore, it can be concluded that the strain-life curve provided a more accurate prediction of fatigue life for welded tubular structures. Although the S-N curve was relatively easy to obtain in practical engineering applications, strain could be measured non-destructively using equipment such as digital image correlation (DIC), which effectively assessed the strain within the specimen and further predicted the fatigue life of structural

components. Additionally, the fatigue life prediction model could be adjusted according to various parameters such as wire type, steel material, and stress ratio, thereby enhancing the universality of the prediction model.

6. Micro-mechanism analysis of failure

The fatigue failure process of welded tubular structures could be divided into three stages: crack initiation, crack propagation, and rapid expansion to the point of failure. In this study, scanning electron microscopy was used to analyze the fracture morphology of welded tubular structure joints under both uniaxial tensile static loading and fatigue testing, as shown in Figs. 16-17. From Fig. 16, it could be observed that the fracture surface of the statically loaded specimen was smooth and neat, with a large number of

dimples, indicating instantaneous fracture of the welded tubular structure joint under static loading.

From Fig. 17, it was evident that the fatigue failure of the tubular originates from the crack initiation zone located at the weld toe, this zone exhibits a flat and smooth morphology, with no obvious plastic deformation, which is a typical feature of fatigue crack initiation under low plastic strain conditions. As the crack propagates, the fracture transitions to a rough fatigue propagation zone with visible fatigue striations, and finally forms a brittle final fracture zone, confirming the 'initiation-propagation-fracture' failure process of the welded joint. The instant fracturing region showed numerous dimples distributed throughout signifying that the relative sliding phenomenon during the fast expansion stage might not easily occur. This suggested a minimal proportion occupied by instantaneous fracturing region over the total fatigue life span which indicated rapid failure after undergoing a period's slow progression towards the final phase post-crack expansion stage. Figs. 16-17 collectively illustrate the progressive fatigue damage process of the welded joint: (1) the crack initiates at the weld toe (stress concentration zone) due to local strain accumulation; (2) the crack propagates stably under cyclic loading, forming fatigue striations with uniform spacing (Fig. 16); (3) the crack propagates unstably until final fracture, forming a rough brittle zone. This process provides clear guidance for anti-fatigue design of welded tubular structures, such as optimizing the weld toe shape through increasing the transition radius to reduce stress concentration or adopting post-weld grinding to smooth the weld surface, which can effectively inhibit fatigue crack initiation at the stress concentration zone and extend the service life of components. In addition, different types of welding wire, steel material, stress ratio, ambient temperature, specimen size and other parameters can be modified subsequently to improve the universality of fatigue life prediction model.

7. Conclusions

This study focused on the welded tubular structure, and combined static tests, fatigue tests, digital image processing, microscopic observations, and theoretical analysis to investigate the fatigue performance and failure mechanisms of the welded tubular structure. The following conclusions were drawn:

(1) The yield strength, tensile strength of welded tubular structures were found to be similar to those of unwelded tubular structures. Both exhibited a failure mode of plastic fracture in the base material, with relatively small strain at the weld seam in welded tubular structures.

(2) Under the action of fatigue load, the welded tubular structure had no obvious yield stage and brittle fracture occurred at the weld. The stress ratio is 0.1, with a stress range of 15.63 MPa to 156.29 MPa, the fatigue life reached 2 million cycles.

(3) The maximum stress in the welded butt joint was concentrated near the weld toe and fusion line, gradually decreasing towards both ends. The peak fatigue strain

occurred in the weld seam area, with the strain values decreasing gradually away from the weld seam. Once a crack appeared at the weld seam, it rapidly propagated and fractured.

(4) Based on the maximum fatigue strain obtained from stress analysis and digital image processing, a predictive formula for the fatigue life of welded pipe structures was proposed. In comparison to S-N curves, the prediction error associated with the strain-life curve was reduced by 7.18%, thereby enabling a more accurate estimation of the fatigue life for this type of structure.

(5) Compared to static fracture, fatigue fracture presented a substantial amount of fatigue striations in the crack propagation zone. During the rapid crack propagation stage, relative sliding was less likely to occur, and the specimen failed rapidly after expansion.

Acknowledgments

This research was funded by National Natural Science Foundation of China (Grant Number.51808265), Natural Science Foundation of the Jiangsu Higher Education Institutions of China (Grant Number.18KJB560005), Key Research and Development of Shandong Province (Grant Number.2019GSF111013), Postgraduate Research & Practice Innovation Program of Jiangsu Province (Grant Number. SJCX24_2548, SJCX24_2556, KYCX24_4135, KYCX24_4138), Jiaxing Public Welfare Research Program Project (Grant Number. 2024AY10011), and Science and Technology Plan Project of Zhejiang Provincial Market Supervision and Administration Bureau in 2025 (Grant Number. ZD2025021).

References

- Acevedo, C. (2011), "Influence of residual stresses on fatigue response of welded tubular K-joints", Ph.D. Dissertation, *Ecole Polytechnique Fédérale de Lausanne*, Lausanne, Switzerland.
- Acevedo, C. and Nussbaumer A. (2012a), "Effect of tensile residual stresses on fatigue crack growth and S-N curves in tubular joints loaded in compression", *Int. J. Fatigue*, **36**(1), 171-180, <https://doi.org/10.1016/j.ijfatigue.2011.07.013>.
- Acevedo, C., Drezet, J.M. and Nussbaumer, A. (2013), "Numerical modelling and experimental investigation on welding residual stresses in large-scale tubular K-joints", *Fatigue Fracture Eng. Mater. Struct.*, **36**(2), 177-185, <https://doi.org/10.1111/j.1460-2695.2012.01712.x>.
- Acevedo, C., Evans, A. and Nussbaumer, A. (2012b), "Neutron diffraction investigations on residual stresses contributing to the fatigue crack growth in ferritic steel tubular bridges", *Int. J. Pressure Vessels Piping*, **95**, 31-38, <https://doi.org/10.1016/j.ijpvp.2012.05.004>.
- ASTM (2013), Standard Test Methods for Tension Testing of Metallic Materials (E8/E8M), ASTM E8/E8M-13; ASTM International, West Conshohocken, PA, USA.
- ASTM (2015), Standard Practice for Conducting Force Controlled Constant Amplitude Axial Fatigue Tests of Metallic Materials (E466), ASTM E466-15, ASTM International, West Conshohocken, PA, USA.
- Barsoum, Z. and Samuelsson, J. (2006), "Fatigue assessment of cruciform joints welded with different methods", *Steel Res. Int.*,

- 77(12), 882-888. <https://doi.org/10.1002/srin.200606476>.
- Chen, X., An, K. and Kim, K.S. (2004), "Low-cycle fatigue of 1Cr-18Ni-9Ti stainless steel and related weld metal under axial, torsional and 90 out-of-phase loading", *Fatigue Fracture Eng. Mater. Struct.*, **27**(6), 439-448, <https://doi.org/10.1111/j.1460-2695.2004.00740.x>.
- Coffin, L.F.J. (1954), "A study of the effects of cyclic thermal stresses on a ductile metal", *J. Fluids Eng.*, **22**(6), 419-606, <https://doi.org/10.1115/1.4015020>.
- Day, W.D. (2011), "Limits on Morrow mean stress correction of Manson-Coffin life prediction models", *ASME Turbo Expo: Turbine Technical Conference & Exposition*, **54662**, 85-92 <https://doi.org/10.1115/GT2011-45444>.
- De Oliveira, J.C., Packer, J.A. and Christopoulos, C. (2008), "Cast steel connectors for circular hollow section braces under inelastic cyclic loading", *J. Struct. Eng.*, **134**(3), 374-383. [https://doi.org/10.1061/\(ASCE\)0733-9445\(2008\)134:3\(374\)](https://doi.org/10.1061/(ASCE)0733-9445(2008)134:3(374)).
- de Oliveira, J.C., Packer, J.A. and Christopoulos, C. (2008), "Cast steel connectors for circular hollow section braces under inelastic cyclic loading", *J. Struct. Eng.*, **134**(3), 374-383. [https://doi.org/10.1061/\(ASCE\)0733-9445\(2008\)134:3\(374\)](https://doi.org/10.1061/(ASCE)0733-9445(2008)134:3(374)).
- Digre, K.A. and Zwerneeman, F. (2012), "Recommended practice for planning, designing and constructing fixed offshore platforms-working stress design", *Insights into using the 22nd edition of API RP 2A*, Offshore Technology Conference, Houston, Texas, USA, April.
- DNV-RP-C203 (2011), *Fatigue Design of Offshore Steel Structures*, Norway: Det Norske Veritas, Oslo, Norway.
- Fu, Y., Tong, L., He, L. and Zhao, X. L. (2016), "Experimental and numerical investigation on behavior of CFRP-strengthened circular hollow section gap K-joints", *Thin-Wall. Struct.*, **102**, 80-97. <https://doi.org/10.1016/j.tws.2016.01.020>.
- Guo, H., Wan, J., Liu, Y. and Hao, J. (2018), "Experimental study on fatigue performance of high strength steel welded joints", *Thin-Wall. Struct.*, **131**, 45-54. <https://doi.org/10.1016/j.tws.2018.06.023>.
- Gurney, T.R. (1991), *The Fatigue Strength of Transverse Fillet Welded Joints: A Study of the Influence of Joint Geometry*, Abington Publishing, England.
- Haedir, J., Bambach, M.R., Zhao, X.L. and Grzebieta, R.H. (2009), "Strength of circular hollow sections (CHS) tubular beams externally reinforced by carbon FRP sheets in pure bending", *Thin-Wall. Struct.*, **47**(10), 1136-1147. <https://doi.org/10.1016/j.tws.2008.10.017>.
- Haldimann-Sturm, S.C. and Nussbaumer, A. (2008), "Fatigue design of cast steel nodes in tubular bridge structures", *Int. J. Fatigue*, **30**(3), 528-537, <https://doi.org/10.1016/j.ijfatigue.2007.03.007>.
- Jiang, H., Chen, Z., Fang, Z., Fang, S., Tu, W., Mo, F. and Liu, J. (2025b), "Rapid hardening high performance concrete (RHHC) for bridge expansion joints: From material properties to interfacial shear performance", *Construct. Build. Mater.*, **458**, 139638. <https://doi.org/10.1016/j.conbuildmat.2024.139638>.
- Jin, G., Chen, Y., Song, G., Fan, Q., Yu, H., Xu, G. and Xu, D. (2023), "Study on fatigue fracture of SW400 fine-grained high-strength steel T-lap joint", *Journal Physics: Conference Series* **2459**(1), 012047, IOP Publishing, Chongqing, China, March.
- Lee, C. and Chang, K. (2013), "Influence of the residual stresses and distortions on the structural behavior of girth-welded cylindrical steel members", *Construct. Build. Mater.*, **41**, 766-776, <https://doi.org/10.1016/j.conbuildmat.2012.12.057>.
- Lee, C.H. and Chang, K.H. (2014), "Comparative study on girth weld-induced residual stresses between austenitic and duplex stainless steel pipe welds", *Appl. Thermal Eng.*, **63**(1), 140-150. <https://doi.org/10.1016/j.applthermaleng.2013.11.001>.
- Lee, C.H., Chang, K.H., Park, K.T., Shin, H.S. and Lee, M. (2014), "Compressive strength of girth-welded stainless steel circular hollow section members: Stub columns", *J. Construct. Steel Res.*, **92**, 15-24. <https://doi.org/10.1016/j.jcsr.2013.09.004>.
- Li, K. and Shao, Y. (2022), "Axial compression performance tests of TT-Type hollow section tube joints strengthened with CFRP", *Space Struct.*, **28**(03), 86-91+76, <https://doi.org/10.13849/j.issn.1006-6578.2022.03.086>.
- Marshall, P.W. (2013), *Design of Welded Tubular Connections: Basis and Use of AWS Code Provisions*, **37**, Elsevier, Houston, Texas, U.S.A.
- Musa, I.A. and Mashiri, F.R. (2019), "Stress concentration factor in concrete-filled steel tubular K-joints under balanced axial load", *Thin-Wall. Struct.*, **139**, 186-195. <https://doi.org/10.1016/j.tws.2019.03.003>.
- Nussbaumer, A. and Costa Borges, L.A. (2008), "Size effects in the fatigue behavior of welded steel tubular bridge joints", *Materialwissenschaft und Werkstofftechnik: Entwicklung, Fertigung, Prüfung, Eigenschaften und Anwendungen technischer Werkstoffe*, **39**(10), 740-748, <https://doi.org/10.1002/mawe.200800356>.
- Nussbaumer, A., Haldimann-Sturm, S.C. and Schumacher, A. (2006), "Fatigue of bridge joints using welded tubes or cast steel node solutions", *Welding World*, **50**, 56-63, <https://doi.org/10.1201/9780203734964-8>.
- Shao, Y., Chen, Z. and Zhou, Z. (2020), "Experimental Investigation on Static Bearing Capacity of Corroded T-Joint Strengthened with CFRP", *J. Civil Eng. Manage.*, **37**(5), 15-19, <https://doi.org/10.13579/j.cnki.2095-0985.2020.05.003>.
- Smith, I.F.C. and Smith, R.A. (1982), "Defects and crack shape development in fillet welded joints", *Fatigue Fracture Eng. Mater. Struct.*, **5**(2), 151-165. <https://doi.org/10.1111/j.1460-2695.1982.tb01231.x>.
- Smith, K.N., Topper, T.H. and Watson, P. (1970), "A stress-strain function for the fatigue of metals (stress-strain function for metal fatigue including mean stress effect)", *J. Mater.*, **5**(4), 767-778.
- Tong, L.W., Chen, K.P., Xu, G.W. and Zhao, X.L. (2019), "Formulae for hot-spot stress concentration factors of concrete-filled CHS T-joints based on experiments and FE analysis", *Thin-Wall. Struct.*, **136**, <https://doi.org/10.1016/j.tws.2018.12.013>.
- Wang L. and Luo, W. (2023), "Analysis of welding temperature field and residual stress in Q355 steel tubular-truss structure", *J. Mater. Sci. Eng.*, **3**(41), 385-390, <https://doi.org/10.14136/j.cnki.ssn1673-2812.2023.03.007>.
- Wu, H.Y., Lei, H.G. and Frank, C.Y. (2021), "Comparison on mechanisms of high-cycle fatigue performance of structural steel exposed to urban industrial atmosphere and laboratory simulated corrosive environment based on infrared thermography", *Int. J. Fatigue*, **145**, 106098, <https://doi.org/10.1016/j.ijfatigue.2020.106098>.
- Yan, R., Yang, W., Ma, P. (2020), "Experimental study on hysteresis performance of plate reinforced circular tube K-joint", *Build. Struct.*, **50**(24), 29-34, <https://doi.org/10.19701/j.jzjg.2020.24.005>.
- Yang, Y., Chen, X., Liu, Y., Xu, T., Chen, P. and He, Z. (2022), "Study on hysteretic performance of welded T-joints circular tube on platform considering seawater corrosion", *Ocean Eng.*, **259**, 111942. <https://doi.org/10.1016/j.oceaneng.2022.111942>.
- Zhao, X.L. and Packer, J.A. (Eds.). (2000), *Fatigue Design Procedure for Welded Hollow Section Joints: Recommendations of IIW Subcommission XV-E*, Elsevier, Cambridge, Abington, UK.
- Zou, S., Chen, R., Wang, H., Fang, Z., Qu, C. and Zhang, C. (2025), "Effect of shear key geometrical dimensions on seismic performance of prefabricated concrete piers with shallow socket connections", *Structure*, **71**, 107975 <https://doi.org/10.1016/j.istruc.2024.107975>.

Zou, S., Wang, H., Fang, S., Fang, Z., Wenliuhan, H., Qu, C. and Zhang, C. (2025a), "Seismic isolation effect and parametric analysis of simply supported beam bridges with multi-level sliding friction adaptive isolation bearing", *Soil Dyn. Earthq. Eng.*, **188**, 109000.
<https://doi.org/10.1016/j.soildyn.2024.109000>.

CC